Journal of Power Sources 238 (2013) 150–156

Contents lists available at SciVerse ScienceDirect

Journal of Power Sources

journal homepage: www.elsevier.com/locate/jpowsour

Morphology controlled high performance supercapacitor behaviour of the Ni–Co binary hydroxide system

Xiang Sun, Gongkai Wang, Hongtao Sun, Fengyuan Lu, Mingpeng Yu, Jie Lian*

Department of Mechanical, Aerospace & Nuclear Engineering, Rensselaer Polytechnic Institute, Troy, NY 12180, USA

HIGHLIGHTS

- Ni–Co binary hydroxide systems with controllable morphologies were fabricated.
- Different morphologies lead to distinct supercapacitive behaviours.
- The performance degradation at high mass loadings can be greatly mitigated.
- Asymmetric cells composed of hydroxides and graphene showed excellent performance.

GRAPHICAL ABSTRACT

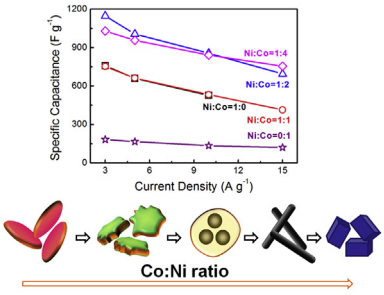

ARTICLE INFO

Article history:
Received 12 December 2012
Received in revised form
26 February 2013
Accepted 16 March 2013
Available online 26 March 2013

Keywords:
Supercapacitor
Nickel hydroxide
Cobalt hydroxide
Nanostructure
Electrochemistry

ABSTRACT

The morphology evolution of the Ni–Co binary hydroxides was studied varying from nanosheets, to nanoplate–nanospheres, to nanorods and to a nanoparticle geometry by simply controlling the Co:Ni ratio in the initial reactant. High capacitances of 1030 F g^{-1} and 804 F g^{-1} can be achieved in the 1-D nanorod morphology at mass loading of 1 mg cm^{-2} and 2.8 mg cm^{-2} at a current density of 3 A g^{-1}, respectively. To demonstrate its practical application, the binary hydroxide electrode was coupled with chemically-reduced graphene (CG) forming an asymmetric supercapacitor in order to improve the potential window and thus energy density. The asymmetric supercapacitor delivers a high energy density of 26.3 Wh kg^{-1} at the power density of 320 W kg^{-1}. The approach of controlling morphology and crystallinity of the binary system for optimizing supercapacitive performance may be applied developing other promising multiply metal hydroxide/oxide systems for supercapacitor applications.

1. Introduction

Development of highly efficient energy storage systems is critical for the expanded utilization of renewable energy resources for fulfilling the energy demand with minimized carbon dioxide emission. Supercapacitors as supplementary to batteries, possess unique advantages including high power density and long term stability, and are being considered as a key component for electrochemical energy storage [1,2]. Current carbon-based supercapacitors are limited with maximum specific capacitance achieved and thus low energy density. It is of technological importance to develop advanced electrode materials with greatly enhanced specific capacitance for achieving desired energy density. One strategy in developing high performance electrode materials with high energy density is based on the pseudo-capacitive materials with multiple valence states, e.g., transition metal oxides/hydroxides, offering complementary surface redox reactions [3]. Among various transition metal oxides/hydroxides, RuO_2 has shown promising capacitance and energy density [4] while its scarcity and high cost limit potential applications.

* Corresponding author. Tel.: +1 518 2766081; fax: +1 518 2766025.
E-mail address: lianj@rpi.edu (J. Lian).

0378-7753/$ – see front matter © 2013 Elsevier B.V. All rights reserved.
http://dx.doi.org/10.1016/j.jpowsour.2013.03.069

Efforts so far have been focused on developing alternative metal hydroxides/oxides which are earth abundant, cost effective and can offer high specific capacitance.

With respect to the intrinsic nature of surface redox reactions, materials for pseudocapacitors must offer a variety of distinct functionalities, including electron and ionic conductivities, active charge storage sites, and desired microstructures. A single component or material rarely exhibits all of these characteristics. Recent developments in nanoscience have enabled a great promise in synthesizing advanced composites of different nano-architectures with multi-functionalities. Binary or ternary nano-composites have been developed, exhibiting enhanced performance and distinct advantages over single element systems [5–11]. Nickel and cobalt are the most studied elements in these systems due to their abundance and high capacitance. The nano-composites consisting of these two electrochemical active elements offer richer charge storage contributions from both nickel and cobalt ions. The most studied system is the binary $NiCo_2O_4$ spinel structure, which is usually produced from the hydrothermal synthesis and thermal decomposition of the Ni and Co hydroxides [12,13]. Promising specific capacitances of 658 F g^{-1} and 694 F g^{-1} at a current density of 1 A g^{-1} have been achieved via manipulating the ratios of the Ni/Co [6,14]. However, the binary hydroxide precursors are less explored as supercapacitor materials. It has been reported that metal hydroxides usually exhibit higher specific capacitances over oxides since the high temperature annealing process to convert hydroxides to oxides may lead to the performance deterioration due to the elimination of surface defects, improved crystallinity, and decrease of the hydrous content [7,15,16]. For example, pronounced capacitances of 1492 F g^{-1} and 1335 F g^{-1} have been achieved in $Co(OH)_2$ and $Ni(OH)_2$ by using zeolite and graphene as hard templates, respectively [17,18]. However, synthesis of highly porous hydroxides especially binary hydroxides with controllable geometries for supercapacitor applications is still less explored. Moreover, the correlation between the morphology and electrochemical performance has not been systematically studied.

In this work, we reported a facile method in synthesizing a highly porous binary Ni–Co hydroxide system with controlled microstructures from nanosheets, to nanoplate encapsulated nanospheres, to nanorods and to a nanoparticle geometry. With the evolution of the morphology, various nano-composites exhibited distinct crystal structures, surface properties, and electrochemical behaviours. By simply tailoring the Ni:Co ratio in the initial reactants, the surface area and specific capacitance of binary composites were greatly enhanced as compared to those of the single component systems. The synthesized binary system, specifically in the nanorod geometry, displays excellent electrochemical performance even at a high current density and high mass loading.

2. Experimental

2.1. Preparation of binary hydroxides

A desired molar mixture of $NiCl_2 \cdot 6H_2O$ and $CoCl_2$, 16 g SDS, 50 g urea, and 30 ml DI water was magnetically stirred at 40 °C for 1 h to obtain a transparent solution. Then the mixture was transferred to an 80 °C oil bath and further reacted for 6 h. The obtained slurry was filtered through a Millipore membrane (0.2 μm), and then dried at 80 °C overnight. The solid was then ground, washed and filtrated repeatedly with water and ethanol to remove the surfactants. The final product was dried in an oven overnight. For synthesis of different Ni–Co binary hydroxides, the initial $NiCl_2 \cdot 6H_2O$ and $CoCl_2$ molar ratio was varied while the total molar of the cations was kept at 0.035 mol.

2.2. Preparation of chemically-reduced graphene (CG)

Graphite oxide (GO) was synthesized by the Hummers method [19]. The well-dispersed graphene solution was prepared according to the procedure reported in our previous publication [20]. Few drops of diluted hydrochloride acid were added dropwise into the graphene colloids and the graphene flakes were immediately coagulated and precipitated out due to the disruption of the electrostatic repulsion [21]. The precipitates were collected by vacuum filtration and then freeze dried in a Labconco free dry system.

2.3. Characterization

The crystal structures and phase composition of the synthesized hydroxides were characterized using XRD (a PANanalytical X-ray diffraction system with Cu radiation at 45 kV, 40 mA). The morphology and microstructure were characterized by a Carl Zeiss Supra 55 SEM and a JEOL 2010 TEM operated at 200 kV. The surface area and pore size distribution were measured using a Quantachrome AUTOSORB-1 instrument, and XPS was recorded on a PHI 5000 Versa Probe system to characterize the valence state of the metal ions.

2.4. Electrochemical measurements

Electrochemical measurements were carried out by a potentiostat VersaSTAT 4 (Princeton Applied Research). The testing system consists of a working electrode (diameter of 1.27 cm^2), a platinum wire (0.02 inch OD) as a counter electrode and a saturated calomel electrode (SCE) as the reference electrode in a 6 M KOH solution. The working electrode was prepared by mixing the active material, carbon black, and polytetrafluoroethylene (PTFE) at a weight ratio of 75:20:5 with small amount of ethanol. After sonication, the slurry was pasted onto circular nickel foam (Novamet Specialty Products Corp.), which was then dried at 80 °C overnight and pressurized. For the assembly of the asymmetric cell, the loading mass ratio of the binary hydroxide (Ni:Co at 1:4) to CG was estimated to be 0.3 based on the specific capacitance obtained from the cycle voltammetry (CV) curves in a three electrode cell (see the results part for details). The electrodes were separated by a porous polypropylene separator (Celgard 3501) and sealed in a coin cell.

3. Results and discussion

The synthesized binary system experiences a phase evolution by changing the ratio of Ni and Co in the reactants. Sodium dodecyl sulphate (SDS) was used as the directing templates and urea as the weak base in promoting mesoporous structures of the nano-hydroxides. While maintaining the ratio of total mole content of the cation, solvent, surfactant, and urea the same, different crystal phases were obtained for the binary system by controlling the amount of Ni and Co in Ni and Co precursors. As observed from the XRD patterns (Fig. 1), the nickel hydroxide hydrate phase (JCPDS 00-022-0444) precipitates out from Ni-enriched binary precursors; while cobalt hydroxide chloride (JCPDS 01-073-2134) can be obtained from Co-enriched precursors with the Ni/Co ratio decreasing below 1:4. For convenience, different synthesized compounds were denoted by the nickel to cobalt ion ratio in the initial reactant.

The structures of layered double hydroxides have been well studied, and it has been found that a counter anion or water is often intercalated into the hydroxide, leading to the formation of nickel hydroxide hydrates with the water complex [22,23]. Using the Co-precursor, cobalt hydroxide chloride compounds were achieved due to the strong electronegativity of chloride ions and its complexation ability with cobalt [24]. pH value plays an important role in controlling the phase formation of the binary hydroxide

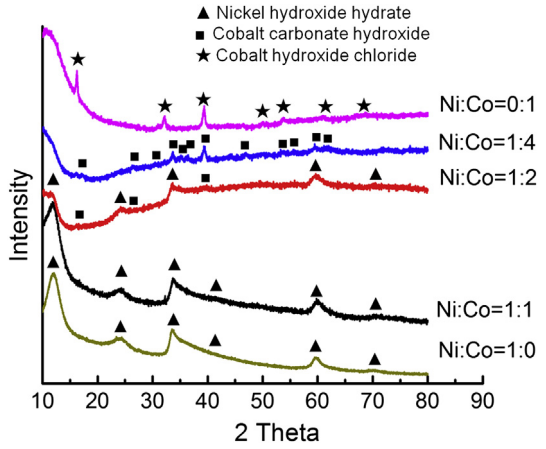

Fig. 1. XRD patterns of nickel–cobalt hydroxides synthesized by controlling the Ni/Co ratios in the initial reactants.

system as the chloride-containing complex was predicted only stable at pH from 3.8 to 8.9. In response to the partial hydrolysis of urea at 80 °C, the slowly-elevated pH value provides sufficient time for the ion exchange and benefits complex rearrangement [25].

Starting from the Ni precursor in the initial reactants, a single nickel hydroxide hydrate phase was obtained. No additional phase was observed upon the addition of Co at the Ni/Co ratio of 1:1. This result suggests that Co was incorporated into the single nickel hydroxide hydrate phase leading to the formation of a possible Ni–Co hydroxide solid solution [26]. This can be evidenced by strong peaks of cobalt binding energy in Co 2p located at 780.7 eV from the XPS spectra (Fig. S1), confirming the presence of the Co–OH bond for a low cobalt addition in the initial reactants [27]. With the Ni to Co ratio decreased to 1:2, cobalt carbonate hydroxide phase (JCPDS 00-048-0083) was precipitated, leading to the mixed phases as confirmed by the X-ray diffraction patterns. As the Ni/Co ratio decreased below 1:4, the formation of carbonate hydroxide is more obvious; while $Co(OH)_3Cl$ crystal peaks began to appear when the Ni/Co ratio was further reduced.

Very interestingly, the distinct crystal phases accompany drastically different morphology evolution by tailoring the initial Ni/Co ratios. The morphology and microstructure of the synthesized binary systems were characterized in details by SEM (Fig. 2) and TEM imaging (Fig. 3). Specifically, the single phase nickel hydroxide hydrate (Ni:Co = 1:0) displays a flower-like feature with nanosheets (Fig. 2a); while the single phase cobalt hydroxide chloride (Ni:Co = 0:1) exhibits a nanoparticle morphology (Fig. 2c). The morphologies are consistent with previous observations [16]. For the solid solution with the Ni to Co ratio of 1:1, the composite still displays a nanosheet geometry (Fig. 3a). As more cobalt ions are involved (Ni:Co = 1:2), nanospheres begin to appear and are encapsulated in the nanoplates (Fig. 3b), corresponding to the mixing phases of cobalt carbonate hydroxide and nickel hydroxide hydrate, respectively. More interestingly, the structures evolved into nanorod morphology as the Ni:Co ratio reaches 1:4 (Figs. 2b and 3c), which is believed to be caused by the Ostwald ripening process, as previously reported in graphene based composites [13] and other one dimensional structures [26]. Note that the nanorod geometry displays a high porous feature with the extensive pores (white contrasts) confined within the rod as shown in the TEM image (Fig. 3c).

The nature of the layered hydroxides and the function of the SDS tend to grow as lamellar structures [28,29]. Attempts in tailoring synthesis parameters, such as varying solvent type and concentration [28,30,31], temperature and control of oxygen atmosphere, in altering morphology have previously been demonstrated [32,33]. From materials chemistry perspective, carbonate anions may act as inhibitors which selectively decrease the crystal growth of a nanorod structure [34]. Similarly, the chloride ions may also have the ability to inhibit the crystal growth, resulting in a distinct morphological evolution. At greater nickel to cobalt ratios in the initial reactants, the hydroxide radicals available for bonding with cobalt ions become depleted, and the competing of hydroxides, carbonate and chloride radicals between Ni and Co hydroxide compounds may affect the morphology, crystallinity and phase of the precipitates. Therefore, the approach of adding a heterogeneous cation (e.g., Ni and Co binary systems) to manipulate the phase composition, crystallinity and microstructure is simple and straightforward. Of particular importance, the binary hydroxides are both electrochemically active. Moreover, the morphology evolution from nanosheet, to nanosphere, to nanorod, to a nanoparticle geometry is controllable by simply adjusting the cation ratio, resulting in distinct supercapacitor behaviours and enabling the direct correlation between the morphology and electrochemical performances.

For effective electrochemical energy storage, mesoporous materials with desired pore structures are essential to facilitate mass transfer of the electrolytes for fast redox reactions [3]. The mesoporous nature of the binary hydroxide was demonstrated by nitrogen adsorption/desorption. As shown in Fig. 4a, the large hysteresis loop in the type IV isotherm indicates the capillary condensation of the mesopore structures. Together with the pore distribution analysis (Fig. 4b) by nonlocal density functional theory (NLDFT), the binary hydroxides all exhibit mesopore structures with the pore size confined at ~4 nm except samples with higher Co concentrations (Ni:Co at 1:4 and 0:1). The textural and morphology evolution were also accompanied by the change of interconnected pores inside particles and the void spaces between the particles. As more cobalt ions (e.g., Ni:Co at 1:4) were added, the sheet morphology was reformed to 1D nanorods, with a broad pore distribution from 2 to 15 nm. In contrast, the nanoparticle morphology for pure cobalt hydroxide chloride (Ni:Co at 0:1) only exhibited external interparticle pores concentrated above 27 nm. As summarized in Fig. S2, the specific surface area increases first and then decreases with decreasing Ni:Co ratios. For the single nickel or cobalt component, the surface area is limited to 30–60 $m^2\ g^{-1}$. The

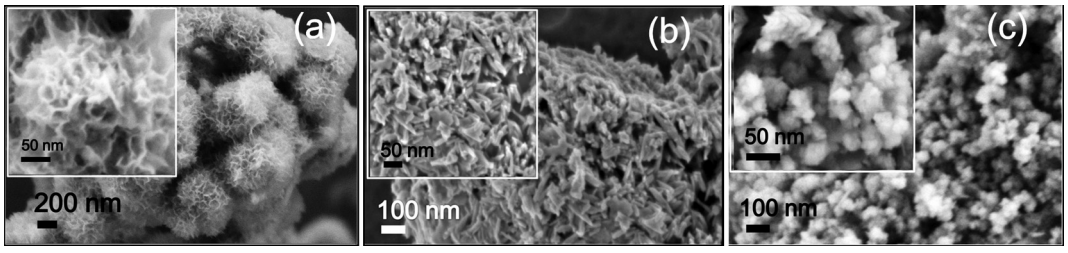

Fig. 2. SEM images showing the morphology evolution from nanosheets, nanorod to nanoparticles at Ni:Co ratios: (a) 1:0, (b) 1:4, (c) 0:1.

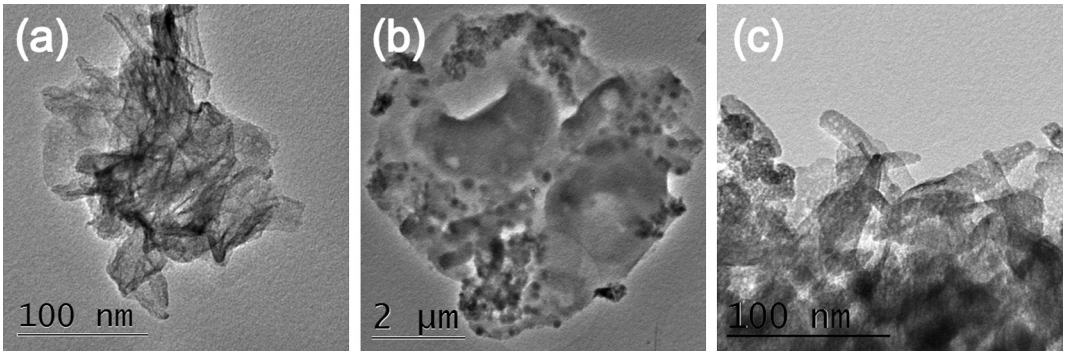

Fig. 3. TEM images of samples at different Ni:Co ratios from (a) 1:1, (b) 1:2, and (c) 1:4.

binary system further opened up the structures, and a maximum surface area of 156.4 m^2 g^{-1} can be achieved at Ni:Co = 1:1. Therefore, the high supercapacitive performance of the binary systems is expected with their desired mesoporous nature satisfying optimal performance requirements for supercapacitor applications [5,35,36].

The redox behaviours of the binary materials were characterized in details by cyclic voltammetry (CV) measured at 10 mV s^{-1}. As shown in Fig. 5a, except the pure cobalt sample, the other four materials displayed evident reversible redox couples. The oxidation peak close to the upper voltage limit corresponds to the Ni phase; while the peak at lower potential is for the Co phase. The redox peaks shifted to negative potential and became broadened with increased cobalt contents. It has been reported that the redox potential of $Co(OH)_2$ to CoOOH transition is more negative than that of $Ni(OH)_2$ to NiOOH transition [17,18]. Thus, the peak shift of our materials can be attributed to the increased cobalt content, which exhibited more cobalt hydroxide-like redox behaviour. The peak broadening is possibly due to the fact that multiple phases exist at intermediate Ni/Co ratios and may display broadened redox features [17]. The overlapping of the redox peaks in binary hydroxides might also contribute to the broadening, demonstrating the benefit of the binary system where more feasible redox states might be contributed by both metal ions. In addition, the Ni phase peak is close to the solvent oxidation, causing the long term instability of the electrodes. By introducing some Co content into the Ni based system, the redox couples could be shifted to lower potential, preventing the solvent oxidation induced performance degradation.

The specific capacitance of the binary system was calculated by using charge/discharge at various current densities. As an example shown in Fig. 5b, the non-linear curve shape again verifies the pseudocapacitance behaviour. The total specific capacitance was calculated by the discharge curve according to the equation $C = I\Delta t/\Delta V$, where I is the current density, Δt is the total discharging time, and ΔV is the voltage range. As summarized in Fig. 5c, specific capacitances of 760, 754, 1147, 1030, and 182 F g^{-1} can be achieved at 3 A g^{-1} and a mass loading of ~1 mg cm^{-2} for samples of Ni:Co = 1:0, 1:1, 1:2, 1:4, and 0:1, respectively. In conjunction with the BET analysis, a close correlation between surface area (Fig. S2) and specific capacitance (Fig. 5c) cannot be identified, indicating the importance of other factors, e.g., morphology, composition and crystallinity, in determining the materials electrochemical performance as electrodes.

Particularly, the specific capacitance generally becomes greater with high concentration Co in the binary compounds with Ni/Co ratios increasing from 1:0 to 1:4, in which the materials experience a drastic morphological evolution from nanosheets to nanorods. The sample Ni:Co at 1:2 has the highest specific capacitance at the current density of 3 A g^{-1}, indicating the most effective charge transfer and high energy storage within the integrated nanospheres/nanoplates geometry. At a high current density of 15 A g^{-1}, the sample Ni:Co at 1:4 displays a greater capacitance of 755 F g^{-1} as compared with that of the sample Ni:Co at 1:2 (695 F g^{-1}). This can be partially attributed to the 1D nanorod morphology and broad pore distribution of the sample Ni:Co (1:4), which may reduce the mass transfer resistance encountered within its larger mesopore structure and moderate the electron hopping between other nanorods. The overall performance of a supercapacitor material is determined by the interplay among various factors including surface area, pore distribution, conductivity, and feasible redox states [5]. At higher charge/discharge rates, the mass transfer and electron conductivity become more dominated, and thus the 1D geometry shows distinct advantages. It was suggested that the hierarchical pore structure can facilitate fast electrolyte and electron transport for performance at high rates, where combined micropores and mesopores can overcome the kinetic limit and enhance the charge storage [37]. The concept was confirmed by the electrochemical impedance measurement (EIS). Fig. S3 compares

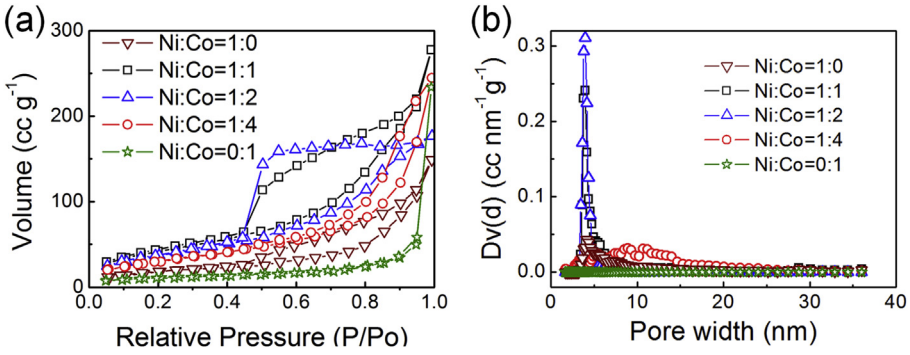

Fig. 4. (a) Nitrogen adsorption/desorption isotherms and (b) NLDFT pore size distribution of binary hydroxides.

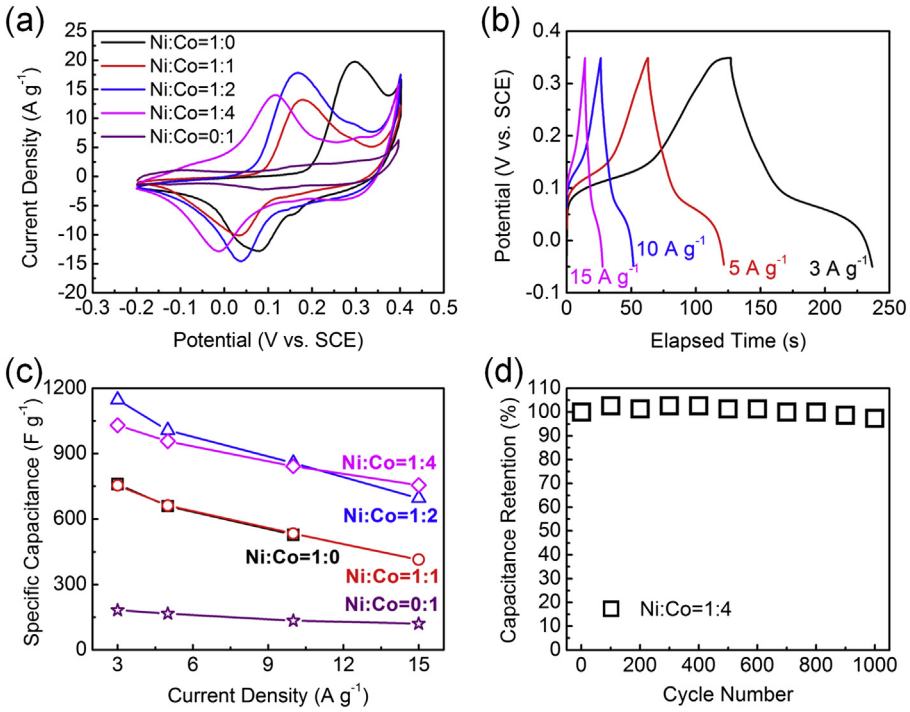

Fig. 5. Electrochemical characterization of the binary Ni–Co hydroxides in 6 M KOH: (a) CV curves obtained at a scan rate of 10 mV s^{-1}, (b) charge/discharge curves obtained at different current densities for the sample Ni:Co = 1:2, (c) specific capacitances of the Ni–Co hydroxides for the samples with different Ni/Co ratios as a function of current density, (d) cycle stability of the sample Ni:Co = 1:4 at 15 A g^{-1}.

the Nyquist plots of sample Ni:Co at 1:1 and 1:4. The spectra were fitted by an equivalent circuit model composed of an electrolyte resistance R_s, charge transfer resistance R_{ct}, pseudo-capacitive element C_p and Warburg diffusion resistance W_1. The charge transfer resistances are 1.75 and 0.47 Ω for Ni:Co at 1:1 and 1:4, respectively. Plus, the Warburg portion tends to become shorter in samples 1:4, which can be correlated with the broad pore distribution and nanorod morphology. Additionally, such sample exhibits excellent cyclability as demonstrated by excellent retention of the specific capacitance (over 97.3%) for the electrode materials after 1000 cycles (Fig. 5d).

The morphology mediated binary Ni/Co compounds also shows great scale up potentials as advanced electrode materials for practical applications. Particularly, the optimization of active materials with respect to the total mass is essentially important for large scale application of energy storage devices [38,39]. Currently, the materials with high performance from the laboratory scale may not be fully realized when they are scaled up towards commercialization, and of particular importance, electrochemical energy storage devices will typically experience performance degradation upon increased mass and thickness of the active materials [40,41]. To demonstrate the strong capability of our binary hydroxides towards practical applications as advanced electrodes, the mass loading effects on their specific capacitance were investigated. As shown in Fig. 6a, the performance of 1D nanorod binary hydroxide (Ni:Co = 1:4) is not significantly affected by the increased mass loading and an impressive capacitance of 804 F g^{-1} is recorded at a high mass loading of 2.8 mg cm^{-2} at a current density of 3 A g^{-1}. In addition, the slightly decreased trend of rate capability is nearly preserved at higher mass loadings. The decrease of the specific capacitance as a function of increased thickness or mass loading typically results from the retarded ion transport and the reduced electron conductivity [39]. Therefore, one dimensional nanorod geometry may provide effective channels for the electron hopping between particles/rods, and allows effective surface utilization for faradic reaction, leading to the highest capacitive performance at

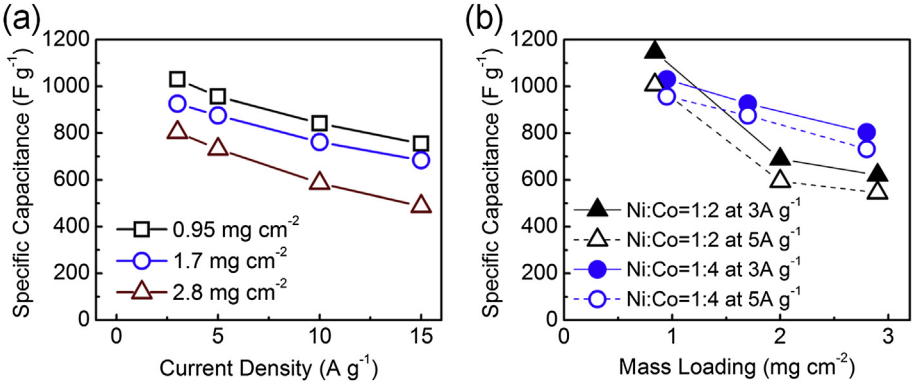

Fig. 6. (a) Specific capacitance of the sample Ni:Co = 1:4 vs current density at various mass loadings, (b) specific capacitance vs mass loadings for the samples Ni:Co = 1:2 and 1:4, in 6 M KOH.

higher mass loadings and greater current densities. As compared with the 1-D nanorod geometry (for the sample Ni:Co = 1:4) (Fig. 6b), the performance degradation due to high mass loading is more severe for the sample Ni:Co = 1:2 with a nanosphere geometry despite its superior performance at ~1 mg cm^{-2}. These results highlight the important role of the morphology control, in which the 1D porous nanorod geometry may enable the effective electron transfer and fast ion transports in order to mitigate the performance degradation at high mass loading for practical applications.

To utilize the redox behaviour of pseudomaterials in an applicable two-electrode system, asymmetric systems by combining a battery-like Faradic electrode and a capacitor type electrode with a notable enhancement in energy density have been extensively studied [42–45]. The symmetric supercapacitor cell suffers from a low operating voltage in aqueous solution limited by the water decomposition at the high potential of 1.2 V [46]. The asymmetric design with the utilization of the different potential windows of the cathode and anode can further expand the operation voltage using aqueous electrolyte and thus improve the system energy density. With respect to the electrolytes used in supercapacitors, aqueous electrolytes have the advantages such as nonflammability, high ionic conductivity, low-cost, and no need for the special assembly atmosphere, as compared to the organic electrolytes [47].

We demonstrated the applicability of the binary hydroxides by forming an asymmetric cell with chemically-reduced graphene (CG). As shown in CV curves (Fig. S4), CG exhibits the typical rectangular shapes from 0 to −1 V without a significant distortion even at a high scan rate of 150 mV s^{-1}. CG and binary hydroxide exhibit a stable voltage window of 1 V and 0.6 V, respectively. Therefore, it is reasonable to expect that the asymmetric cell constructed by these two components will have a stable operation window of at least 1.5 V. To fully deliver the redox peaks of the binary hydroxides, the charges stored in the cathode should be balanced by charges in the anode. Thus, the optimized mass ratio of the sample Ni:Co = 1:4 to CG is 0.3 based on the equation $q = C \times m \times \Delta E$, where q is the charges stored on each electrode, ΔE is the potential range, m is the mass of each electrode, and C is the specific capacitance (760 F g^{-1} for Ni:Co = 1:4 and 136 F g^{-1} for CG at 10 mV s^{-1}).

Fig. 7a shows the CV curve of the asymmetric cell with an optimized cathode/anode mass ratio of 0.3 in 6 M KOH at various scan rates. The asymmetric supercapacitor shows an ideal capacitive behaviour with a nearly rectangular CV curve with a stable potential window of 1.5 V even at a high scan rate of 150 mV s^{-1}. The good linear relation from the various galvanostatic charge–discharge curves (Fig. 7b) also indicates its good capacitive response. The specific capacitance of the asymmetric cell is calculated from the integration of the CV curves based on the equation $C = (\int I dt)/m\Delta V$, where I is the current response, dt is the scan time interval, m is the total mass of active materials in both electrodes (anodes and cathodes) and ΔV is the voltage range of each scan.

As displayed in Fig. 7c, a maximum capacitance of 84.3 F g^{-1} (per cell capacitance) can be achieved at a scan rate of 5 mV s^{-1}, which is 2.3 times those for NiO and AC asymmetric cells [48]. The higher potential window of the asymmetric cell also provides extra advantages for improved energy and power densities. As summarized in the Ragone plot (Fig. 7d), the asymmetric supercapacitor exhibits an energy density of 26.3 Wh kg^{-1} at a power density of 320 W kg^{-1} and still maintains 14.7 Wh kg^{-1} at a power of 5.3 kW kg^{-1}, higher than the best performing MnO_2 asymmetric cell (7 Wh kg^{-1} at 5 kW kg^{-1}) [43] in neutral electrolyte and NiO asymmetric cells (15–20 Wh kg^{-1}) [48,49] in alkaline electrolyte. It should be noted that the energy and power densities are plotted based on the total mass of the active materials instead of the total system weight in the Ragone plot. The energy and power densities can be further improved by forming composites with conductive substrates [13], or coupling a better double layer electrode (porous graphene) [45] or pseudomaterial [50]. Moreover, the asymmetric cell showed excellent cycle stability (Fig. S5).

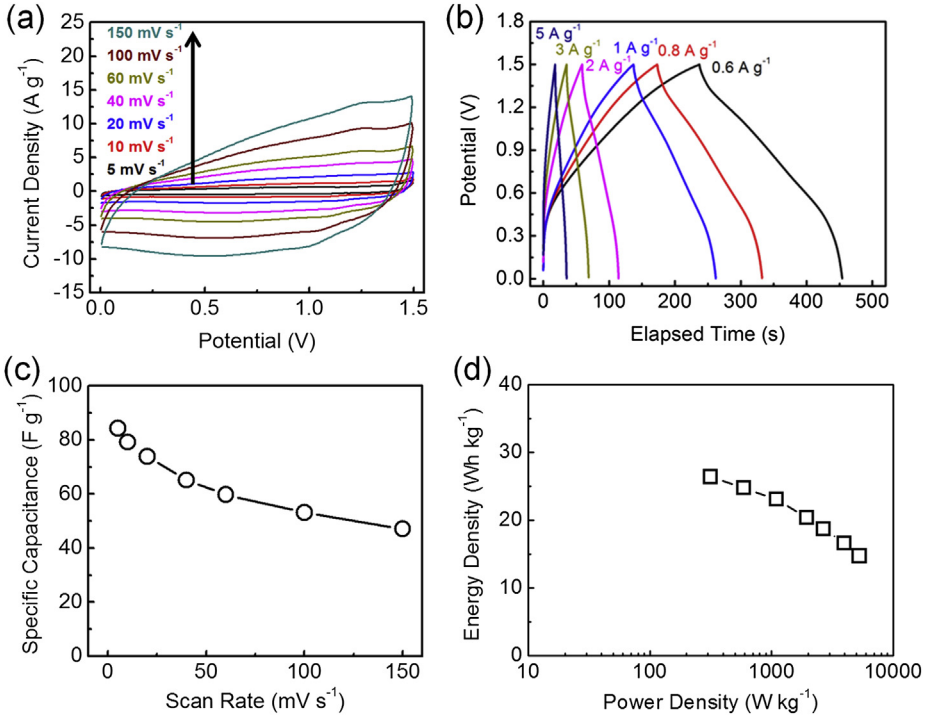

Fig. 7. Electrochemical characterization of the Ni:Co = 1:4 and CG asymmetric cell: (a) CV curves obtained at various scan rates showing the stable voltage window of 1.5 V, (b) charge/discharge curves obtained at different current densities, (c) specific capacitances of the asymmetric cell as a function of scan rates, (d) Ragone plot of energy and power densities of the asymmetric supercapacitor, in 6 M KOH.

4. Conclusions

In summary, we fabricated Ni–Co binary hydroxide systems with controllable morphologies from nanosheets, to nanoplates–nanospheres, to nanorods, and to a nanoparticle geometry by simply tailoring the Ni and Co cation ratios in the initial reactants. The highly open structure of the binary hydroxides with drastically different morphologies significantly affects the electrochemical performance of binary hydroxides for advanced electrode materials. An extremely high capacitance of 1030 F g^{-1} was achieved for the nanorod morphology at the current density of 3 A g^{-1} at a mass loading of 1 mg cm^{-2}. Of particular importance, the performance degradation at high mass loadings can be greatly mitigated by utilizing the open structure of the nanorod morphology in which an impressive capacitance of 804 F g^{-1} can be achieved at the current density of 3 A g^{-1} and the mass loading of 2.8 mg cm^{-2}. These results highlight a generic approach for developing advanced electrodes upon manipulation of the morphology of the binary system, which in turn governs various factors including conductivity, surface area, pore structure and feasible redox states, for optimizing supercapacitive performance. Such binary systems, for the first time, exhibit amazing performance, particularly at high mass loading, and may stimulate other promising multiply metal hydroxide/oxide systems for supercapacitor applications.

Acknowledgements

This work was financially supported by a NSF Career Award under the Award of DMR 1151028.

Appendix A. Supplementary data

Supplementary data related to this article can be found at http://dx.doi.org/10.1016/j.jpowsour.2013.03.069.

References

[1] A. Burke, J. Power Sources 91 (2000) 37–50.
[2] J.R. Miller, A.F. Burke, ECS Interface 17 (2008) 53.
[3] P. Simon, Y. Gogotsi, Nat. Mater. 7 (2008) 845–854.
[4] C.C. Hu, W.C. Chen, K.H. Chang, J. Electrochem. Soc. 151 (2004) A281–A290.
[5] T.Y. Wei, C.H. Chen, H.C. Chien, S.Y. Lu, C.C. Hu, Adv. Mater. 22 (2010) 347–351.
[6] H.L. Wang, Q.M. Gao, L. Jiang, Small 7 (2011) 2454–2459.
[7] S.G. Kandalkar, H.M. Lee, S.H. Seo, K. Lee, C.K. Kim, J. Mater. Sci. 46 (2011) 2977–2981.
[8] K.X. He, X.G. Zhang, J. Li, Electrochim. Acta 51 (2006) 1289–1292.
[9] X.M. Liu, Y.H. Zhang, X.G. Zhang, S.Y. Fu, Electrochim. Acta 49 (2004) 3137–3141.
[10] H.L. Wang, Q.M. Gao, J. Hu, J. Power Sources 195 (2010) 3017–3024.
[11] G. Wang, X. Sun, F. Lu, Q. Yu, C. Liu, J. Lian, J. Solid State Chem. 185 (2012) 172–179.
[12] H.W. Wang, Z.A. Hu, Y.Q. Chang, Y.L. Chen, H.Y. Wu, Z.Y. Zhang, Y.Y. Yang, J. Mater. Chem. 21 (2011) 10504–10511.
[13] J.W. Xiao, S.H. Yang, J. Mater. Chem. 22 (2012) 12253–12262.
[14] J.W. Xiao, S.H. Yang, RSC Adv. 1 (2011) 588–595.
[15] R.S. Jayashree, P.V. Kamath, G.N. Subbanna, J. Electrochem. Soc. 147 (2000) 2029–2032.
[16] X. Sun, G.K. Wang, J.Y. Hwang, J. Lian, J. Mater. Chem. 21 (2011) 16581–16588.
[17] L. Cao, F. Xu, Y.Y. Liang, H.L. Li, Adv. Mater. 16 (2004) 1853–1857.
[18] H.L. Wang, H.S. Casalongue, Y.Y. Liang, H.J. Dai, J. Am. Chem. Soc. 132 (2010) 7472–7477.
[19] W.S. Hummers, R.E. Offeman, J. Am. Chem. Soc. 80 (1958) 1339.
[20] G.K. Wang, X. Sun, F.Y. Lu, H.T. Sun, M.P. Yu, W.L. Jiang, C.S. Liu, J. Lian, Small 8 (2012) 452–459.
[21] D. Li, M.B. Muller, S. Gilje, R.B. Kaner, G.G. Wallace, Nat. Nanotechnol. 3 (2008) 101–105.
[22] V. Rives, Layered Double Hydroxides: Present and Future, Nova Publishers, Hauppauge, NY, 2001.
[23] D.G. Evans, R.C.T. Slade, Struct. Bond. 119 (2006) 1–87.
[24] Z.G. Zhao, F.X. Geng, J.B. Bai, H.M. Cheng, J. Phys. Chem. C 111 (2007) 3848–3852.
[25] J.R. Neilson, B. Schwenzer, R. Seshadri, D.E. Morse, Inorg. Chem. 48 (2009) 11017–11023.
[26] X.P. Shen, J.Q. Sun, G.X. Wang, J. Park, K.M. Chen, Mater. Res. Bull. 45 (2010) 766–771.
[27] B. Schwenzer, K.M. Roth, J.R. Gomm, M. Murr, D.E. Morse, J. Mater. Chem. 16 (2006) 401–407.
[28] R. Qiao, X.L. Zhang, R. Qiu, J.C. Kim, Y.S. Kang, Chem. Eur. J. 15 (2009) 1886–1892.
[29] W.W. Zhou, J.P. Liu, T. Chen, K.S. Tan, X.T. Jia, Z.Q. Luo, C.X. Cong, H.P. Yang, C.M. Li, T. Yu, Phys. Chem. Chem. Phys. 13 (2011) 14462–14465.
[30] H.T. Cui, M. Zayat, D. Levy, J. Nanopart. Res. 11 (2009) 1331–1338.
[31] C.C. Li, X.M. Yin, Q.H. Li, L.B. Chen, T.H. Wang, Chem. Eur. J. 17 (2011) 1596–1604.
[32] F.D. Wu, Y. Wang, J. Mater. Chem. 21 (2011) 6636–6641.
[33] L.Q. Zhang, A.K. Dutta, G. Jarero, P. Stroeve, Langmuir 16 (2000) 7095–7100.
[34] R. Xu, H.C. Zeng, J. Phys. Chem. B 107 (2003) 12643–12649.
[35] T. Brezesinski, J. Wang, S.H. Tolbert, B. Dunn, Nat. Mater. 9 (2010) 146–151.
[36] C.C. Hu, K.H. Chang, M.C. Lin, Y.T. Wu, Nano Lett. 6 (2006) 2690–2695.
[37] D.-W. Wang, F. Li, M. Liu, G.Q. Lu, H.-M. Cheng, Angew. Chem. Int. Ed. 47 (2008) 373–376.
[38] M.D. Stoller, R.S. Ruoff, Energy Environ. Sci. 3 (2010) 1294–1301.
[39] L.B. Hu, W. Chen, X. Xie, N.A. Liu, Y. Yang, H. Wu, Y. Yao, M. Pasta, H.N. Alshareef, Y. Cui, ACS Nano 5 (2011) 8904–8913.
[40] D. Choi, G.E. Blomgren, P.N. Kumta, Adv. Mater. 18 (2006) 1178–1182.
[41] L.B. Hu, J.W. Choi, Y. Yang, S. Jeong, F. La Mantia, L.F. Cui, Y. Cui, Proc. Natl. Acad. Sci. U. S. A. 106 (2009) 21490–21494.
[42] Q. Wang, Z.H. Wen, J.H. Li, Adv. Funct. Mater. 16 (2006) 2141–2146.
[43] Z.S. Wu, W.C. Ren, D.W. Wang, F. Li, B.L. Liu, H.M. Cheng, ACS Nano 4 (2010) 5835–5842.
[44] Z.J. Fan, J. Yan, T. Wei, L.J. Zhi, G.Q. Ning, T.Y. Li, F. Wei, Adv. Funct. Mater. 21 (2011) 2366–2375.
[45] J. Yan, Z.J. Fan, W. Sun, G.Q. Ning, T. Wei, Q. Zhang, R.F. Zhang, L.J. Zhi, F. Wei, Adv. Funct. Mater. 22 (2012) 2632–2641.
[46] C. Liu, F. Li, L.P. Ma, H.M. Cheng, Adv. Mater. 22 (2010) E28–E62.
[47] C.J. Xu, H.D. Du, B.H. Li, F.Y. Kang, Y.Q. Zeng, J. Electrochem. Soc. 156 (2009) A435–A441.
[48] D.W. Wang, F. Li, H.M. Cheng, J. Power Sources 185 (2008) 1563–1568.
[49] H. Inoue, Y. Namba, E. Higuchi, J. Power Sources 195 (2010) 6239–6244.
[50] H.L. Wang, Y.Y. Liang, T. Mirfakhrai, Z. Chen, H.S. Casalongue, H.J. Dai, Nano Res. 4 (2011) 729–736.